Influence of the Spatial Distribution of Molecular Magnetic Moments on the Radiation Characteristics of Rotating Permanent Magnet Antennas

Tiantian Li, Bin Li*, and Jin Meng

National Key Laboratory of Electromagnetic Energy, Naval University of Engineering, Wuhan 430033, Hubei, China

ABSTRACT: Taking into account the radiation characteristics of rotating permanent magnet antennas, the influence of the spatial distribution of molecular magnetic moments on the radiation characteristics was verified by performing theoretical calculations and simulations. First, the magnetic field distribution of arbitrarily shaped permanent magnets was derived based on the Biot-Savart Law, and the concentration degree of the molecular magnetic moments to the connection of the two magnetic poles and the comprehensive performance evaluation index were defined. The theoretical model to analyze the performance of permanent magnets was also established as above. Second, by controlling volume and rotational inertia to be the same, three types of permanent magnets were calculated. Finally, the optimization design process was proposed. Three preferable solutions were systematically compared and analyzed taking radially magnetized cylindrical permanent magnets as an example. Our work provides valuable insights into the design of mechanical antenna radiation sources.

1. INTRODUCTION

Low frequency electromagnetic waves are widely used in both communication and navigation [1, 2]. However, traditional transmitting antenna is limited by electric size and low radiation efficiency [3], which has reached the development limit at this stage. To realize the miniaturization and light weight of low-frequency transmitting antennas, since the Defense Advanced Research Projects Agency (DARPA) proposed the "A MEchanically Based Antenna" project in 2017 [4], permanent magnets have become the preferred object for the fabrication of mechanical antennas due to the rather high magnetic energy density [5]. Furthermore, rotating permanent magnet antennas are expected to generate efficient ELF-VLF radiation with portable systems [6].

To evaluate the radiation characteristics of mechanical antennas, theoretical studies have been conducted in the literature from different perspectives [7–12]. In the form of mechanical motions, the rotating mechanical antenna can achieve two times the radiated power output of the vibrating mechanical antenna [13]. The equations of the electromagnetic field distribution of the rotating permanent magnets can be summarized by analogy with the circular current [14]. It has been demonstrated that the maximum radiation direction of the cylindrical rotating permanent magnet antenna is its radial direction, and the minimum radiation direction is the direction of the rotation axis. Besides, with an appropriate reduction of the radius and increase of the height, the rotational inertia can be reduced, and the need for motor torque can be reduced [15]. However, a general method based on the intrinsic factors of radiating sources

is lacking to enhance the radiation strength of mechanical antennas.

Along these lines, in this work, the molecular magnetic moment method was used to obtain the expressions for the magnetic field of arbitrarily shaped permanent magnets by calculating the current density on the surface of permanent magnets. Moreover, the expressions for the magnetic field components of cylindrical, spherical, and cuboid permanent magnets were obtained. Simulations were also performed to verify the validity and feasibility of the proposed method. Considering the requirements for motor torque [15], the comprehensive performance evaluation index was defined to provide theoretical insights for obtaining a comprehensive performance of the different types and different sizes of permanent magnets.
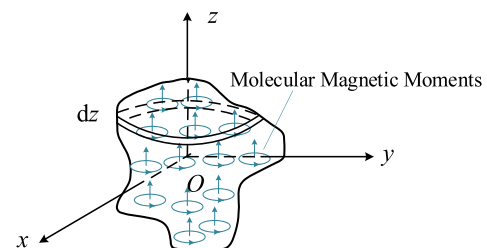

FIGURE 1. An arbitrarily shaped permanent magnet.

2. PERFORMANCE EVALUATION MODELING

2.1. Arbitrarily Shaped Permanent Magnets

As shown in Figure 1, a three-dimensional right-angle coordinate system was constructed with the center of mass of an arbi-

trarily shaped permanent magnet as the origin. Its magnetism can be explained by an atomic model, where each molecule (or atom) of the permanent magnet is equated to a toroidal current, which is called molecular current, and its magnetic moment is called molecular magnetic moment, defined as [16]

$$\mathbf{p}_m = i\Delta\mathbf{S} \tag{1}$$

where i is the molecular current, and $\Delta\mathbf{S}$ is defined as $\Delta\mathbf{S} = \mathbf{e}_n\Delta S$, referring to the area element vector enclosed by the molecular current, whose direction $\mathbf{e}_n$ is in a right-handed spiral relationship with the direction of i.

The vector sum of molecular magnetic moments per unit volume of magnetic medium is magnetization intensity vector, which can be defined as follows:

$$\mathbf{M} = \lim_{\Delta V \to 0} \frac{\sum_i \mathbf{p}_{mi}}{\Delta V} \tag{2}$$

where $\mathbf{p}_{mi}$ denotes the magnetic moment of the ith molecule in the volume ΔV.

Assuming that the permanent magnet is uniformly magnetized along the z direction, the magnetization intensity vector can be expressed as follows:

$$\mathbf{M} = \mathbf{e}_z M \tag{3}$$

where $\mathbf{e}_z$ is the z-coordinate unit vector, and M stands for the magnitude of the magnetization intensity vector $\mathbf{M}$.

When a magnetic medium is magnetized, a macroscopic current distribution, which is called magnetization current, may appear inside and on the surface. The magnetization current density inside a permanent magnet that is uniformly magnetized along the z-direction can be estimated as follows [16]:

$$\mathcal{J}_M = \nabla \times \mathbf{M} = \mathbf{0} \tag{4}$$

Parallel to the xOy plane, a thin layer element with a thickness of $\mathrm{d}z$ was taken from the permanent magnet, and a current element $I\mathrm{d}\mathbf{l}$ was taken from a source point (x, y, z) at the boundary of the thin layer. The current density vector of the magnetization surface can be calculated as follows [16]:

$$\mathcal{J}_{SM} = \mathbf{M} \times \mathbf{e}_n \tag{5}$$

where $\mathbf{e}_n$ is the normal unit vector of the surface of the permanent magnet.

Taking a line element $\mathrm{d}s$ perpendicular to the direction of current flow, the magnitude of the bound current on the boundary can be expressed as follows:

$$I = \mathcal{J}_{SM}\mathrm{d}s \tag{6}$$

where $\mathcal{J}_{SM}$ is the magnitude of the magnetization surface current density vector $\mathcal{J}_{SM}$.

According to the Biot-Savart Law, the magnetic induction produced by the current element $I\mathrm{d}\mathbf{l}$ at any point (x_1, y_1, z_1) outside the permanent magnet can be estimated as follows:

$$\mathrm{d}\mathbf{B}_1 = \frac{\mu_0}{4\pi}\frac{I\mathrm{d}\mathbf{l} \times \mathbf{R}}{|\mathbf{R}|^3} = \frac{\mu_0}{4\pi}\frac{J_{SM}\mathrm{d}s \cdot \mathrm{d}\mathbf{l} \times \mathbf{R}}{|\mathbf{R}|^3}$$

$$= \frac{\mu_0 J_{SM}\mathrm{d}s}{4\pi}\frac{\begin{vmatrix} \mathbf{i} & \mathbf{j} & \mathbf{k} \\ \mathrm{d}x & \mathrm{d}y & 0 \\ x_1 - x & y_1 - y & z_1 - z \end{vmatrix}}{\left[(x_1 - x)^2 + (y_1 - y)^2 + (z_1 - z)^2\right]^{\frac{3}{2}}}$$

$$= \frac{\mu_0 J_{SM}\mathrm{d}s}{4\pi}\frac{\begin{array}{c}(z_1 - z)\,\mathrm{d}y\mathbf{i} - (z_1 - z)\,\mathrm{d}x\mathbf{j} \\ + [(y_1 - y)\,\mathrm{d}x - (x_1 - x)\,\mathrm{d}y]\,\mathbf{k}\end{array}}{\left[(x_1 - x)^2 + (y_1 - y)^2 + (z_1 - z)^2\right]^{\frac{3}{2}}} \tag{7}$$

The magnetic induction generated by the entire thin layer at the point (x_1, y_1, z_1) can be expressed as follows:

$$\mathrm{d}\mathbf{B} = \oint_L \mathrm{d}\mathbf{B}_1$$

$$= \oint_L \frac{\mu_0 J_{SM}\mathrm{d}s}{4\pi}\frac{\begin{array}{c}(z_1 - z)\,\mathrm{d}y\mathbf{i} - (z_1 - z)\,\mathrm{d}x\mathbf{j} \\ + [(y_1 - y)\,\mathrm{d}x - (x_1 - x)\,\mathrm{d}y]\,\mathbf{k}\end{array}}{\left[(x_1 - x)^2 + (y_1 - y)^2 + (z_1 - z)^2\right]^{\frac{3}{2}}} \tag{8}$$

The magnetic induction generated by the entire permanent magnet at the point (x_1, y_1, z_1) can be calculated as follows:

$$\mathbf{B} = \int \mathrm{d}\mathbf{B}$$

$$= \int\oint_L \frac{\mu_0 J_{SM}\mathrm{d}s}{4\pi}\frac{\begin{array}{c}(z_1 - z)\,\mathrm{d}y\mathbf{i} - (z_1 - z)\,\mathrm{d}x\mathbf{j} \\ + [(y_1 - y)\,\mathrm{d}x - (x_1 - x)\,\mathrm{d}y]\,\mathbf{k}\end{array}}{\left[(x_1 - x)^2 + (y_1 - y)^2 + (z_1 - z)^2\right]^{\frac{3}{2}}} \tag{9}$$

According to Faraday's Law of Electromagnetic Induction, the induced electromotive force is proportional to the changing rate of the magnetic flux in time through the area enclosed by the circuit. Likewise, the magnitude of the magnetic moment of a permanent magnet is constant, and to produce radiation, the direction of the magnetic moment must be changed during the motion. Taking into account that the magnetic flux density reaches its maximum at the two poles and is opposite in direction, and the magnitudes of the rotational inertia directly affect the motor torque required to rotate the antenna [15], the rotation axis should be perpendicular to the line of the two magnetic poles combined with practical application. At the same time, the moment of inertia of the permanent magnet is minimized, and the problem can be simplified to compare the magnetic flux density on the extension line of the two magnetic poles.

For the same permanent magnet, the rotational inertia is different when the rotation axis is different, and the rotational inertia for the x-axis can be calculated as follows:

$$J_x = \int_V r^2\mathrm{d}m \tag{10}$$

where $\mathrm{d}m$ represents the mass of a mass point on the permanent magnet, and r stands for the distance from the mass point to the rotation axis.

Similarly, the concentration degree of the molecular magnetic moments to the connection of two magnetic poles can be defined as follows:

$$K = \frac{1}{\int_V r_1^2 \mathrm{d}m_1} \tag{11}$$

where $\mathrm{d}m_1$ is the mass of a molecule in the permanent magnet, and r_1 states the distance between the molecule and the line connecting the two magnetic poles.

Different types and sizes of permanent magnets have different radiation characteristics and rotational inertias. To facilitate quantitative comparison, the comprehensive performance evaluation index can be defined as follows:

$$H = \frac{K}{J} \tag{12}$$

where K denotes the concentration degree of the molecular magnetic moments to the connection of two magnetic poles, and J represents the rotational inertia of the permanent magnet.

2.2. Magnetic Field Distribution of Different Types of Permanent Magnets

2.2.1. Cylindrical Permanent Magnets

As can be seen in Figure 2, the height of the cylindrical permanent magnet is h, and the radius is R. The geometric center is located at the origin of the right-angle coordinate system, and the axis coincides with the x-axis. Parallel to the xOy plane, a thin layer element with a thickness of $\mathrm{d}z$ is taken. According to the calculation method presented in Section 2.1, the magnitude of the bound current density on the cylinder bottom surface is M, and the magnitude of the bound current density on the side of the cylinder is $M\cos\phi$. Additionally, the magnitude of the bound current on the entire thin layer boundary is $M\mathrm{d}z$, whose direction is in a right-handed spiral relationship with $\mathbf{e}_z$. The $x, y,$ and z components of the magnetic flux density at any point (x_1, y_1, z_1) outside the permanent magnet can be estimated as follows:

$$B_x = \frac{\mu_0 M}{4\pi} \int_{-R}^{R} \mathrm{d}z \int_{-\sqrt{R^2-z^2}}^{\sqrt{R^2-z^2}}$$

$$\left\{ \frac{1}{\left[(x_1 - h/2)^2 + (y_1 - y)^2 + (z_1 - z)^2 \right]^{\frac{3}{2}}} \right.$$

$$\left. - \frac{1}{\left[(x_1 + h/2)^2 + (y_1 - y)^2 + (z_1 - z)^2 \right]^{\frac{3}{2}}} \right\} (z_1 - z)\,\mathrm{d}y \tag{13}$$

$$B_y = \frac{\mu_0 M}{4\pi} \int_{-R}^{R} dz \int_{-h/2}^{h/2}$$

$$\left\{ \frac{1}{\left[(x_1 - x)^2 + \left(y_1 - \sqrt{R^2 - z^2}\right)^2 + (z_1 - z)^2 \right]^{\frac{3}{2}}} \right.$$

$$\left. - \frac{1}{\left[(x_1 - x)^2 + \left(y_1 + \sqrt{R^2 - z^2}\right)^2 + (z_1 - z)^2 \right]^{\frac{3}{2}}} \right\} (z_1 - z)\mathrm{d}x \tag{14}$$

$$B_z = \frac{\mu_0 M}{4\pi} \int_{-R}^{R} \mathrm{d}z \int_{-\sqrt{R^2-z^2}}^{\sqrt{R^2-z^2}}$$

$$\frac{-(x_1 - h/2)}{\left[(x_1 - h/2)^2 + (y_1 - y)^2 + (z_1 - z)^2 \right]^{\frac{3}{2}}}$$

$$+ \frac{x_1 + h/2}{\left[(x_1 + h/2)^2 + (y_1 - y)^2 + (z_1 - z)^2 \right]^{\frac{3}{2}}} \, \mathrm{d}y$$

$$+ \frac{\mu_0 M}{4\pi} \int_{-R}^{R} \mathrm{d}z \int_{-h/2}^{h/2}$$

$$\frac{-\left(y_1 - \sqrt{R^2 - z^2}\right)}{\left[(x_1 - x)^2 + \left(y_1 - \sqrt{R^2 - z^2}\right)^2 + (z_1 - z)^2 \right]^{\frac{3}{2}}}$$

$$+ \frac{y_1 + \sqrt{R^2 - z^2}}{\left[(x_1 - x)^2 + \left(y_1 + \sqrt{R^2 - z^2}\right)^2 + (z_1 - z)^2 \right]^{\frac{3}{2}}} \, \mathrm{d}x \tag{15}$$

The comprehensive performance evaluation index can be defined as follows:

$$H = \frac{24}{\pi^2 \rho^2 R^6 h^2 (3R^2 + h^2)} \tag{16}$$

where ρ represents the density of the permanent magnet.

2.2.2. Spherical Permanent Magnets

As can be seen in Figure 3, the radius of the spherical permanent magnet is R. The center of the sphere is located at the origin of the right-angle coordinate system. Parallel to the xOy plane, a thin layer element with a thickness of $\mathrm{d}z$ is taken. The magnitude of the bound current density on the surface is $M\sin\theta$. Additionally, the magnitude of the bound surface current is $M\mathrm{d}z$, whose direction is in a right-handed spiral relationship with $\mathbf{e}_z$. The $x, y,$ and z components of the magnetic flux density at any point (x_1, y_1, z_1) outside the permanent magnet can be expressed as follows:

$$B_x = \frac{\mu_0 M}{4\pi} \int_{-R}^{R} dz \int_{-\sqrt{R^2-z^2}}^{\sqrt{R^2-z^2}}$$

$$\left\{ \frac{1}{\left[\left(x_1 - \sqrt{R^2 - y^2 - z^2}\right)^2 + (y_1 - y)^2 + (z_1 - z)^2 \right]^{\frac{3}{2}}} \right.$$
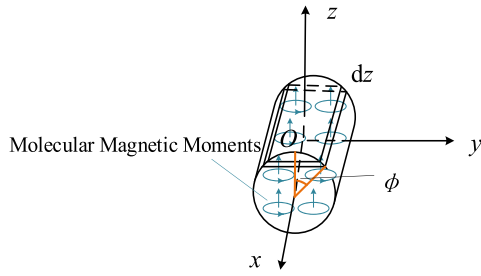
FIGURE 2. Schematic illustration of a cylindrical permanent magnet.

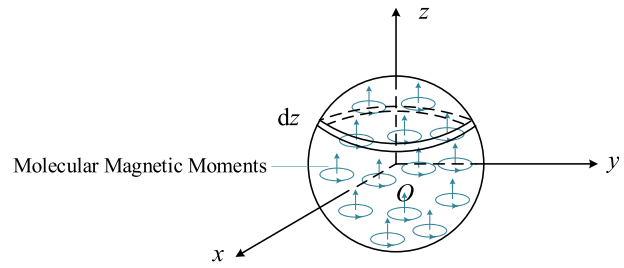**FIGURE 3**. Schematic illustration of a spherical permanent magnet.

$$-\frac{1}{\left[\left(x_1+\sqrt{R^2-y^2-z^2}\right)^2+(y_1-y)^2+(z_1-z)^2\right]^{\frac{3}{2}}}\Bigg\}$$
$$(z_1-z)\,\mathrm{d}y \tag{17}$$

$$B_y=\frac{\mu_0 M}{4\pi}\int_{-R}^{R}dz\int_{-\sqrt{R^2-z^2}}^{\sqrt{R^2-z^2}}$$

$$\Bigg\{\frac{1}{\left[(x_1-x)^2+\left(y_1-\sqrt{R^2-x^2-z^2}\right)^2+(z_1-z)^2\right]^{\frac{3}{2}}}$$
$$-\frac{1}{\left[(x_1-x)^2+\left(y_1+\sqrt{R^2-x^2-z^2}\right)^2+(z_1-z)^2\right]^{\frac{3}{2}}}\Bigg\}$$
$$(z_1-z)\,\mathrm{d}x \tag{18}$$

$$B_z=\frac{\mu_0 M}{4\pi}\int_{-R}^{R}dz\int_{-\sqrt{R^2-z^2}}^{\sqrt{R^2-z^2}}$$

$$\frac{-\left(x_1-\sqrt{R^2-y^2-z^2}\right)}{\left[\left(x_1-\sqrt{R^2-y^2-z^2}\right)^2+(y_1-y)^2+(z_1-z)^2\right]^{\frac{3}{2}}}$$
$$+\frac{x_1+\sqrt{R^2-y^2-z^2}}{\left[\left(x_1+\sqrt{R^2-y^2-z^2}\right)^2+(y_1-y)^2+(z_1-z)^2\right]^{\frac{3}{2}}}\,\mathrm{d}y$$

$$+\frac{\mu_0 M}{4\pi}\int_{-R}^{R}dz\int_{-\sqrt{R^2-z^2}}^{\sqrt{R^2-z^2}}$$

$$\frac{-\left(y_1-\sqrt{R^2-x^2-z^2}\right)}{\left[(x_1-x)^2+\left(y_1-\sqrt{R^2-x^2-z^2}\right)^2+(z_1-z)^2\right]^{\frac{3}{2}}}$$
$$+\frac{y_1+\sqrt{R^2-x^2-z^2}}{\left[(x_1-x)^2+\left(y_1+\sqrt{R^2-x^2-z^2}\right)^2+(z_1-z)^2\right]^{\frac{3}{2}}}\,\mathrm{d}x \tag{19}$$

The comprehensive performance evaluation index can be defined as follows:

$$H=\frac{225}{64\pi^2\rho^2 R^{10}} \tag{20}$$
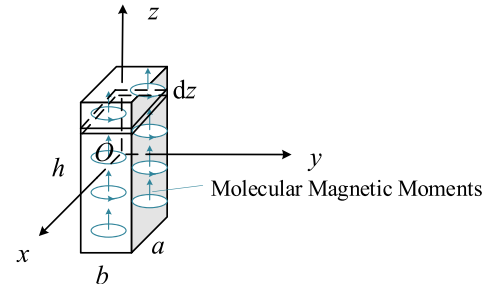

FIGURE 4. Schematic illustration of a cuboid permanent magnet.

2.2.3. Cuboid Permanent Magnets

As can be ascertained from Figure 4, the length, width, and height of the cuboid permanent magnet are a, b, and h, respectively. The geometric center is located at the origin of the right-angle coordinate system, and the direction of the height is parallel to the z-axis. Parallel to the xOy plane, a thin layer element with a thickness of $\mathrm{d}z$ is also taken. The magnitude of the bound current density on the surface is M, and the magnitude of the bound surface current is $M\mathrm{d}z$, whose direction is in a right-handed spiral relationship with $\mathbf{e}_z$. The x, y, and z components of the magnetic flux density at any point (x_1,y_1,z_1) outside the permanent magnet can be defined as follows:

$$B_x=\frac{\mu_0 M}{4\pi}\int_{-h/2}^{h/2}\mathrm{d}z\int_{-b/2}^{b/2}$$

$$\Bigg\{\frac{1}{\left[(x_1-a/2)^2+(y_1-y)^2+(z_1-z)^2\right]^{\frac{3}{2}}}$$
$$-\frac{1}{\left[(x_1+a/2)^2+(y_1-y)^2+(z_1-z)^2\right]^{\frac{3}{2}}}\Bigg\}(z_1-z)\,\mathrm{d}y \tag{21}$$

$$B_y=\frac{\mu_0 M}{4\pi}\int_{-h/2}^{h/2}\mathrm{d}z\int_{-a/2}^{a/2}$$

$$\Bigg\{\frac{1}{\left[(x_1-x)^2+(y_1-b/2)^2+(z_1-z)^2\right]^{\frac{3}{2}}}$$

$$-\frac{1}{\left[(x_1-x)^2+(y_1+b/2)^2+(z_1-z)^2\right]^{\frac{3}{2}}}\Bigg\}(z_1-z)\,\mathrm{d}x \quad (22)$$

$$B_z = \frac{\mu_0 M}{4\pi}\int_{-h/2}^{h/2}\mathrm{d}z\int_{-b/2}^{b/2}$$

$$\frac{-(x_1-a/2)}{\left[(x_1-a/2)^2+(y_1-y)^2+(z_1-z)^2\right]^{\frac{3}{2}}}$$

$$+\frac{x_1+a/2}{\left[(x_1+a/2)^2+(y_1-y)^2+(z_1-z)^2\right]^{\frac{3}{2}}}\,\mathrm{d}y$$

$$+\frac{\mu_0 M}{4\pi}\int_{-h/2}^{h/2}\mathrm{d}z\int_{-a/2}^{a/2}$$

$$\frac{-(y_1-b/2)}{\left[(x_1-x)^2+(y_1-b/2)^2+(z_1-z)^2\right]^{\frac{3}{2}}}$$

$$+\frac{y_1+b/2}{\left[(x_1-x)^2+(y_1+b/2)^2+(z_1-z)^2\right]^{\frac{3}{2}}}\,\mathrm{d}x \quad (23)$$

The comprehensive performance evaluation index can be expressed as follows:

$$H = \frac{144}{\rho^2 a^2 b^2 h^2 \left(a^2+b^2\right)\left(b^2+h^2\right)} \quad (24)$$

3. CALCULATION AND SIMULATION

The NdFeB permanent magnet was selected as the radiating source of the mechanical antenna here, and the residual magnetic flux density was $B_r = 1.4\,\mathrm{T}$. Taking the cuboid NdFeB permanent magnet as an example, according to the relationship between the surface bound current density and the residual magnetic flux density [3], the surface bound current density was calculated as $J_m = B_r/\mu_0 \approx 1114084.6\,\mathrm{A/m}$, and the magnitude of the magnetization intensity vector was $M = 1114084.6\,\mathrm{A/m}$ from Equation (5). Under the saturation magnetization condition, the magnitudes of the magnetization intensity vector of the cylindrical and spherical permanent magnets were the same as that of cuboid permanent magnets. To compare and verify the radiation characteristics of the different forms of permanent magnet antennas, cylindrical and spherical permanent magnets of the same material were selected for comparison.

3.1. Radiation Characteristics of Different Types of Permanent Magnets

Based on the theory in Section 2, the magnitudes of the magnetic induction at the desired field points were calculated by performing numerical integration. Cuboid, cylindrical, and spherical permanent magnet simulation models were built in the COMSOL MULTIPHYSICS software package to verify the correctness of the theoretical results. The surrounding medium space was set as a spherical vacuum domain, and the NdFeB permanent magnet model was uniformly magnetized along the z-direction. To improve the calculation efficiency, different degrees of refinement meshes were constructed for the permanent magnets and the vacuum domain, respectively. The radiation field strength is proportional to the magnetic moment provided by the antenna, and the magnetic moment of the permanent magnet can be defined as follows [15]:

$$m_{\mathrm{magnet}} = \frac{B_r}{\mu_0}\cdot V \quad (25)$$

where B_r represents the residual magnetic flux density, $\mu = 4\pi\times 10^{-7}$ H/m the vacuum permeability, and V the volume of the permanent magnet.

To compare the radiation characteristics of the different types of permanent magnets, the permanent magnet magnetic moment (in practice, the volume) and the rotational inertia were set to be the same by the variable-controlling method.

Table 1 lists the dimensional parameters of the different types of permanent magnets, taking the density value $\rho = 7.5\,\mathrm{g/cm^3}$. Table 2 gives the magnitudes of the magnetic induction on the extension of the line connecting the two magnetic poles at a distance. As can be seen, the magnitudes of the magnetic induction of cuboid and spherical permanent magnets were slightly larger than that of the cylindrical permanent magnets. The comprehensive performance evaluation indexes were maximum for spherical and minimum for cuboid, implying that for the same volume, spherical permanent magnets were able to maintain a larger radiation field strength when the rotational inertia is smaller.

Figure 5 displays the magnitudes of the magnetic flux density on the extension line of the two magnetic poles at the close distance, which is the same as the law at the far distance, and the values of the corresponding positions of the cuboid and spherical permanent magnets were slightly larger than those of the cylindrical permanent magnets.

According to the calculated and simulated results, when the magnetic moments are the same, there are differences in the magnitudes of the magnetic flux density on the extension line of the two poles of different types of permanent magnets. This effect indicates that the radiation performance is not only related to the magnitudes of the whole magnetic moment of the permanent magnet on the macroscopic level, but also connected with the distribution of the molecular magnetic moments on the microscopic level, and it is more obvious at close distances.

In fact, it can be assumed that permanent magnets of different types but the same volume contain the same number of molecular magnetic moments, and there is also a conservation relationship between the numbers of the emitted magnetic induction lines on the closed sphere that surrounds the permanent magnets. Although in this work only the magnitudes of the magnetic flux density on the extension line of the two magnetic poles were compared, the difference reflects the change in the spatial distribution of the magnetic induction lines of the various types of permanent magnets. Table 2 and Figure 5 show that

TABLE 1. Dimensional parameters of the different types of permanent magnets.

No.	Type	Geometric Dimensions	Rotational Inertia
1	Cuboid	$b = h = 62.13\,\text{mm}$ $a = 69.95\,\text{mm}$ $V = 270016.58\,\text{mm}^3$	$J = 1.3029 \times 10^{-3}\,\text{kg·m}^2$
2	Cylindrical	$R = 35.87\,\text{mm}$ $h = 66.80\,\text{mm}$ $V = 270015.74\,\text{mm}^3$	$J = 1.3028 \times 10^{-3}\,\text{kg·m}^2$
3	Spherical	$R = 40.1\,\text{mm}$ $V = 270098.22\,\text{mm}^3$	$J = 1.3030 \times 10^{-3}\,\text{kg·m}^2$

TABLE 2. The magnitudes of magnetic induction on the extension line of two magnetic poles at a distance for different types of permanent magnets.

| Type	Distance	1 m	10 m	100 m	1000 m	H/ kg^{-2}·m^{-4}
Cuboid	Theoretical Value/ T	6.0149×10^{-5}	6.0164×10^{-8}	6.0164×10^{-11}	6.0164×10^{-14}	5.1958×10^5
	Simulation Value/ T	5.9113×10^{-5}	5.8140×10^{-8}	5.4520×10^{-11}	5.9466×10^{-14}	
Cylindrical	Theoretical Value/ T	5.7484×10^{-5}	5.7505×10^{-8}	5.7505×10^{-11}	5.7505×10^{-14}	5.4651×10^5
	Simulation Value/ T	5.8576×10^{-5}	5.7322×10^{-8}	5.4567×10^{-11}	5.0613×10^{-14}	
Spherical	Theoretical Value/ T	6.0182×10^{-5}	6.0182×10^{-8}	6.0182×10^{-11}	6.0182×10^{-14}	5.8899×10^5
	Simulation Value/ T	5.9599×10^{-5}	6.1819×10^{-8}	6.0047×10^{-11}	6.1206×10^{-14}	
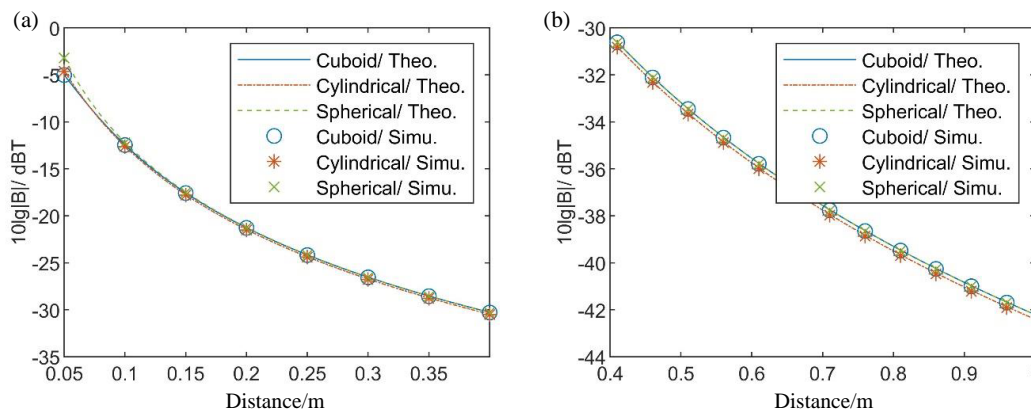
FIGURE 5. The magnitudes of magnetic induction on the extension of the line connecting the two magnetic poles at the near distance for different types of permanent magnets. (a) 0.05–0.4 m, (b) 0.41–1 m.

the laws of the magnetic flux density are the same for the different types of permanent magnets at long and close distances.

3.2. Radiation Characteristics of Different Size Permanent Magnets of the Same Type

In practical applications, when optimizing the design of permanent magnets is used in mechanical antennas, the constraints to be considered include equipment size, motor torque, radiation field intensity, rotational stability, etc. The proposed optimization process is described in Figure 6.

Taking the cylindrical permanent magnets as an example, the upper limit of the radiation source size was set to 120 mm, and three groups of preferred solutions were selected according to the optimization process. The permanent magnet size parameters are presented in Table 3, taking the density value

TABLE 3. Parameters related to the different sizes of cylindrical permanent magnets.

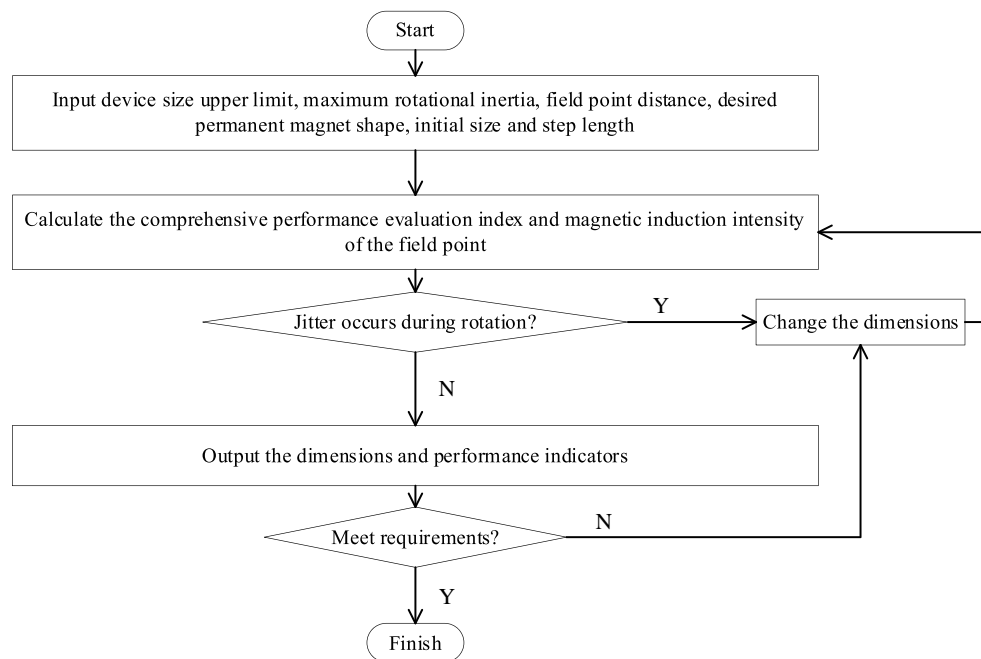| No.	Geometric Dimensions	Rotational Inertia
1	$R = 26.76\,\text{mm}$ $h = 120\,\text{mm}$ $V = 269962.44\,\text{mm}^3$	$J = 7.2495 \times 10^4\,\text{kg·m}^2$
2	$R = 32.74\,\text{mm}$ $h = 80.18\,\text{mm}$ $V = 270005.91\,\text{mm}^3$	$J = 1.0853 \times 10^3\,\text{kg·m}^2$
3	$R = 46.35\,\text{mm}$ $h = 40\,\text{mm}$ $V = 269966.17\,\text{mm}^3$	$J = 2.1749 \times 10^3\,\text{kg·m}^2$

FIGURE 6. Optimization process of the permanent magnet size.

TABLE 4. Performance comparison of the different sizes of cylindrical permanent magnets at long distances.

No.	Magnitudes of Magnetic Flux Density/T				$H/\text{T·kg}^{-2}\text{·m}^{-4}$
	1 m	10 m	100 m	1000 m	
1	4.1321×10^{-5}	4.1461×10^{-8}	4.1462×10^{-11}	4.1462×10^{-14}	4.9404×10^5
2	5.0888×10^{-5}	5.0933×10^{-8}	5.0933×10^{-11}	5.0933×10^{-14}	5.6611×10^5
3	8.9246×10^{-5}	8.9242×10^{-8}	8.9242×10^{-11}	8.9242×10^{-14}	3.3873×10^5

$\rho = 7.5\,\text{g/cm}^3$. Table 4 calculates the magnitudes of the magnetic flux density on the extension line of the two magnetic poles.

Under the current constraints, permanent magnet No. 1 exhibited the smallest rotational inertia; permanent magnet No. 2 had the largest comprehensive performance evaluation index; and permanent magnet No. 3 possessed a larger radiation field strength. The radii of permanent magnets Nos. 1, 2, and 3 increased in turn. Although the magnitudes of the magnetic flux density at the same distance also increased in turn, the com-

prehensive performance indexes showed a tendency to increase and then decrease due to the simultaneous increase in rotational inertia. Thereby, it can be inferred that permanent magnets of the same type and the same magnetic moment have different radiation characteristics and requirements for motor torque at different sizes, which requires comprehensive consideration.

Figure 7 plots the magnitudes of the magnetic induction on the extension of the line connecting the two magnetic poles at close distances for cylindrical permanent magnets of different sizes, which is reflected as increasing in order with the number.
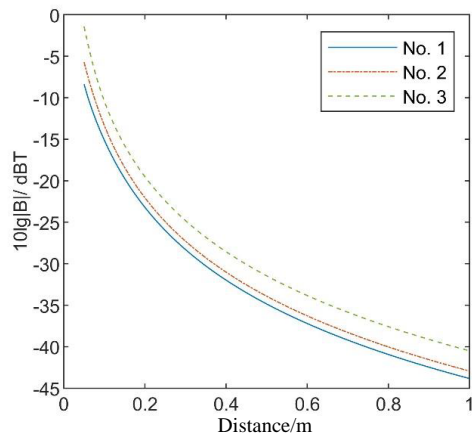
FIGURE 7. Magnitudes of magnetic induction on the extension line of two magnetic poles at a close distance of cylindrical permanent magnets of different sizes.

For the same type, same volume, and different sizes of permanent magnets, the enhanced concentration of the molecular magnetic moments around the two pole lines leads to a larger magnitude of the magnetic induction on the extension of the two pole lines. On top of that, the increased concentration of the mass elements around the rotation axis yields a smaller rotational inertia. Since the two poles are perpendicular to the rotation axis, the distribution of the mass elements, i.e., the size of the permanent magnet, needs to be comprehensively optimized.

The differences in the magnitudes of magnetic induction in Figure 7 are more pronounced than those in Figure 5 because of the greater dissimilarities in the concentration of the molecular magnetic moments with respect to the two pole lines of the three permanent magnets used on a microscopic level. This effect is reflected in greater differences in the size of the cylinders on a macroscopic level.

The volume of the permanent magnet used in Section 3.2 was the same as that in Section 3.1. However, the cylindrical permanent magnet with the largest comprehensive performance evaluation index still has a smaller index than the spherical permanent magnet.

4. CONCLUSION

In this work, the influence of the molecular magnetic moment distribution on the radiation characteristics of a rotating permanent magnet antenna was thoroughly studied. The external magnetic field distribution of the permanent magnets was theoretically derived. The concentration degree of the molecular magnetic moments to the connection of two magnetic poles and the comprehensive performance evaluation index was also defined.

The magnitudes of the magnetic induction on the extension line of the two poles of cuboid, cylindrical, and spherical permanent magnets with typical dimensions were calculated and consistent with the simulation results. From the calculated and simulated outcomes, the following conclusions can be drawn: (1) As far as the magnetic flux density is concerned, the values

of cuboid and spherical were slightly larger than the cylindrical permanent magnets, and the differences increased with the distance. Compared with the radiation field intensity that is proportional to the magnetic moment provided by the antenna as pointed out in work [15], it was demonstrated that the radiation characteristics are also related to the spatial distribution of the molecular magnetic moments inside the antenna. (2) Taking three radially magnetized cylindrical permanent magnets with the same volume but different dimensions as an example, the existence of a larger radius leads to a bigger magnetic flux density on the extension line of the two magnetic poles. However, the comprehensive performance evaluation index may be reduced because of the larger rotational inertia.

REFERENCES

[1] Fawole, O. C. and M. Tabib-Azar, "An electromechanically modulated permanent magnet antenna for wireless communication in harsh electromagnetic environments," *IEEE Transactions on Antennas and Propagation*, Vol. 65, No. 12, 6927–6936, Dec. 2017.

[2] Burch, H. C., A. Garraud, M. F. Mitchell, R. C. Moore, and D. P. Arnold, "Experimental generation of ELF radio signals using a rotating magnet," *IEEE Transactions on Antennas and Propagation*, Vol. 66, No. 11, 6265–6272, Nov. 2018.

[3] Shi, W., Q. Zhou, and B. Liu, "Performance analysis of spinning magnet as mechanical antenna," *Acta Physica Sinica*, Vol. 68, No. 18, Sep. 2019.

[4] Ding, H., *Darpa Mechanical Antenna Project May Set Off a Military Communications Revolution*, 71–73, Conmilit, 2017.

[5] Zhang, F., Z. Gong, S. Wang, Y. Ji, and G. Fang, "A rotating-permanent-magnet array for ULF through-the-sea magnetic communications," *IEEE Transactions on Antennas and Propagation*, Vol. 71, No. 3, 2300–2310, Mar. 2023.

[6] Golkowski, M., J. Park, J. Bittle, B. Babaiahgari, R. A. L. Rorrer, and Z. Celinski, "Novel mechanical magnetic shutter antenna for ELF/VLF radiation," in *2018 IEEE Antennas and Propagation Society International Symposium on Antennas and Propagation & USNC/URSI National Radio Science Meeting*, 65–66, Boston, Ma, Jul. 2018.

[7] Dong, C., Y. He, M. Li, C. Tu, Z. Chu, X. Liang, H. Chen, Y. Wei, M. Zaeimbashi, X. Wang, H. Lin, Y. Gao, and N. X. Sun, "A portable very low frequency (VLF) communication system based on acoustically actuated magnetoelectric antennas," *IEEE Antennas and Wireless Propagation Letters*, Vol. 19, No. 3, 398–402, Mar. 2020.

[8] Kemp, M. A., M. Franzi, A. Haase, E. Jongewaard, M. T. Whittaker, M. Kirkpatrick, and R. Sparr, "A high Q piezoelectric resonator as a portable VLF transmitter," *Nature Communications*, Vol. 10, No. 1, 1715–1721, Apr. 2019.

[9] Cui, Y., M. Wu, X. Song, Y.-P. Huang, Q. Jia, Y.-F. Tao, and C. Wang, "Research progress of small low-frequency transmitting antenna," *Acta Physica Sinica*, Vol. 69, No. 20, 1–13, Oct. 2020.

[10] Fereidoony, F., S. P. M. Nagaraja, J. P. D. Santos, and Y. E. Wang, "Efficient ULF transmission utilizing stacked magnetic pendulum array," *IEEE Transactions on Antennas and Propagation*, Vol. 70, No. 1, 585–597, Jan. 2022.

[11] Rezaei, H., V. Khilkevich, S. Yong, D. S. Stutts, and D. Pommerenke, "Mechanical magnetic field generator for communication in the ULF range," *IEEE Transactions on Antennas and Propagation*, Vol. 68, No. 3, 2332–2339, Mar. 2020.

[12] Liu, Y., S. Gong, Q. Liu, and M. Hou, "A mechanical transmitter for undersea magnetic induction communication," *IEEE Transactions on Antennas and Propagation*, Vol. 69, No. 10, 6391–6400, Oct. 2021.

[13] Zhou, Q., F. Q. Yao, W. Shi, Z. Y. Hao, H. Zheng, B. Liu, and H. E. Panfeng, "Research on mechanism and key technology of mechanical antenna for a low-frequency transmission," *Scientia Sinica Technologica*, Vol. 50, No. 1, 69–84, 2020.

[14] Bickford, J. A., A. E. Duwel, M. S. Weinberg, R. S. McNabb, D. K. Freeman, and P. A. Ward, "Performance of electrically small conventional and mechanical antennas," *IEEE Transactions on Antennas and Propagation*, Vol. 67, No. 4, 2209–2223, Apr. 2019.

[15] Zhang, F., F. Sun, X. Qu, Z. Gong, Y. Ji, and G. Fang, "Research on low frequency communication technology based on rotating permanent magnet," *Journal of Electronics & Information Technology*, Vol. 44, No. 6, 2151–2157, Jun. 2022.

[16] Hayt, W. H., Jr. and J. A. Buck, *Engineering Electromagnetics*, 8th ed., McGraw-Hill, New York, NY, USA, 2010.